Available online at www.sciencedirect.com

ScienceDirect

International Journal of Solids and Structures 44 (2007) 6382–6397

INTERNATIONAL JOURNAL OF SOLIDS AND STRUCTURES

www.elsevier.com/locate/ijsolstr

Strain gradient crystal plasticity analysis of a single crystal containing a cylindrical void

Ulrik Borg [a,*], Jeffrey W. Kysar [b]

[a] *Department of Mechanical Engineering, Solid Mechanics, Technical University of Denmark, Kgs. Lyngby DK-2800, Denmark*
[b] *Department of Mechanical Engineering, Fu Foundation School of Engineering and Applied Science, Columbia University, 500 West 120th Street, New York, NY 10027, USA*

Received 20 December 2006; received in revised form 20 February 2007
Available online 25 February 2007

Abstract

The effects of void size and hardening in a hexagonal close-packed single crystal containing a cylindrical void loaded by a far-field equibiaxial tensile stress under plane strain conditions are studied. The crystal has three in-plane slip systems oriented at the angle 60° with respect to one another. Finite element simulations are performed using a strain gradient crystal plasticity formulation with an intrinsic length scale parameter in a non-local strain gradient constitutive framework. For a vanishing length scale parameter the non-local formulation reduces to a local crystal plasticity formulation. The stress and deformation fields obtained with a local non-hardening constitutive formulation are compared to those obtained from a local hardening formulation and to those from a non-local formulation. Compared to the case of the non-hardening local constitutive formulation, it is shown that a local theory with hardening has only minor effects on the deformation field around the void, whereas a significant difference is obtained with the non-local constitutive relation. Finally, it is shown that the applied stress state required to activate plastic deformation at the void is up to three times higher for smaller void sizes than for larger void sizes in the non-local material.

Keywords: Void; Strain gradient plasticity; Single crystal

1. Introduction

It is well accepted that crack growth in many ductile materials occurs by the mechanisms of void nucleation, growth and coalescence. Voids typically nucleate from second phase particles which exist within the material. The sizes of the voids are often of the order of one micrometer. Elastic–plastic continuum analyses to model the subsequent growth of the voids have traditionally employed isotropic material properties (see, e.g., Koplik and Needleman (1988) and Tvergaard (1990)). However, since the size of the voids is often smaller

* Corresponding author. Tel.: +45 4525 4262; fax: +45 4593 1475.
E-mail address: ub@mek.dtu.dk (U. Borg).

0020-7683/$ - see front matter
doi:10.1016/j.ijsolstr.2007.02.032

than the grain size in a polycrystalline material, it is more appropriate to assume anisotropic elastic–plastic properties.

There are two regimes in which plasticity around a void in an anisotropic single crystal have been studied analytically. The first is for voids that are sufficiently small so that the continuum plasticity approximation is not valid. Several authors (e.g., Stevens et al., 1972; Lubarda et al., 2004; Ahn et al., 2006) have considered the interaction between voids and individual dislocation loops for cylindrical voids as well as spherical voids. The focus of these studies was to calculate the applied stress state at which discrete dislocation loops are nucleated from the void, which leads to void growth.

The other regime is for void sizes for which the continuum approximation is valid. Recent studies (Kysar et al., 2005; Gan and Kysar, 2007) have used continuum anisotropic slip line theory to derive the stress and deformation fields associated with a cylindrical void in a single face centered cubic crystal as well as a hexagonal close packed crystal, along with related experimental and numerical studies by Gan et al. (2006). The constitutive properties considered for the analytical studies are rigid, ideally plastic. The studies have shown that there are angular regions around such voids within which slip on single slip systems occurs. The stress states were also derived and it was shown that the average pressure necessary to activate plastic deformation around a void in a face centered cubic crystal can be up to 50% higher than that for an isotropic material, although for a hexagonal close packed material the average pressure necessary to activate plastic deformation around the void is approximately the same as for isotropic plastic materials. These analyses are applicable for voids which are significantly larger than the voids treated by discrete dislocation plasticity.

The emphasis of the present study is to extend the anisotropic slip line studies, which assume ideal plasticity, to material constitutive models which account for hardening of plastic slip systems and void size effects. Two different material models will be considered. The first includes strain hardening which is typically associated with the creation and accumulation of so-called statistically stored dislocations. This type of strain hardening is implemented in a local constitutive formulation which has no intrinsic length scale. The other material model includes strain gradient effects which are typically associated with the segregation of so-called geometrically necessary dislocations. This type of material model is implemented in a non-local constitutive formulation – or strain gradient plasticity formulation – which has an intrinsic length scale. Simulations are performed with both types of material models and the resulting stress and deformation fields are compared to each other as well as to the analytical solution for plastic deformation around voids.

The formulation of the continuum single crystal plasticity theory with no intrinsic length scale is similar to that employed by Peirce et al. (1983). The strain gradient formulation employed in this study is as presented by Borg (in press). The basic formulation is equivalent to that of Gurtin (2002) and the constitutive equations are based on the theory by Fleck and Hutchinson (2001). A representative material length scale of about 5 μm has been estimated by Fleck et al. (1994) from fitting experimental data on a copper wire torsion test to strain gradient plasticity theory results. Also, Fredriksson and Gudmundson (2005) have compared results by a strain gradient plasticity theory with experimental results, which have given estimates of the material length scale ranging from 0.45 to 2.7 μm. These estimates are performed with strain gradient formulations different from the one used in the present study, however the present length scale is also expected to be on that order. Furthermore, recent work which compares simulations which utilize strain gradient crystal plasticity theory employed in the present study to discrete dislocation plasticity simulations suggests the material length scale to be approximately 0.33 μm (Hussein et al., in press).

For the local case there is no length scale so the size of the void does not enter into consideration. However, for the non-local case the size of the void must be specified. The two void sizes to be considered have radii $r_0/l = 10$ and $r_0/l = 1$, where r_0 and l are the initial radius and the length scale of the constitutive relationship, respectively.

The effect of hardening behaviors within the framework of a non-local constitutive model and also the framework of a local constitutive model are investigated separately. It will be shown that the addition of hardening to the local model mainly reduces the amount of slip which occurs near a void; the extent and boundaries of the single slip angular sectors are not affected. The non-local formulation, on the other hand, introduces a significant change in the extent and boundaries of the single slip sectors. In fact, the sector structure changes significantly so that regions of double slip develop. It is also shown that the critical stress

to activate plastic deformation around the void is up to three times higher for the smaller void size than for the larger void size, at least for the non-local constitutive formulation chosen for this study.

This paper is organized as follows. Section 2 discusses the material model used in this study. This will be followed by a discussion of the numerical implementation of the material model in Section 3. The results of the simulations are presented in Section 4. Concluding discussions are in Section 5.

2. Material model

The material model used for this study is a strain gradient crystal plasticity theory for finite strains proposed by Borg (in press). The theory is based on the constitutive framework of the isotropic strain gradient plasticity theory by Fleck and Hutchinson (2001) including ideas from the finite strain version by Niordson and Redanz (2004), and with the basic formulation equivalent to the formulation of Gurtin (2002). In the absence of strain gradients the model reduces to conventional crystal plasticity theory by, e.g., Peirce et al. (1983). For simplicity, the following summary of the model is only valid for small strains, even though a formulation that allows for finite strains has been used for the analyses.

In crystal plasticity the quantitative description of plastic deformation is based on crystallographic shearing that represents dislocation motion along specific slip systems. A slip system is described by its unit lattice vectors $s_i^{(\alpha)}$ and $m_i^{(\alpha)}$, where $s_i^{(\alpha)}$ is the slip direction and $m_i^{(\alpha)}$ is the direction normal to the slip plane. By use of the classical Schmid orientation tensor

$$\mu_{ij}^{(\alpha)} = \tfrac{1}{2}(s_i^{(\alpha)} m_j^{(\alpha)} + s_j^{(\alpha)} m_i^{(\alpha)}) \tag{1}$$

the overall macroscopic plastic strain rate components can be expressed by the slip $\gamma^{(\alpha)}$ along slip system (α) as

$$\dot{\epsilon}_{ij}^{p} = \sum_{\alpha} \dot{\gamma}^{(\alpha)} \mu_{ij}^{(\alpha)} \tag{2}$$

To account for the effect of increased material hardening due to the presence of geometrically necessary dislocations caused by plastic strain gradients, the plastic dissipation rate does not only depend on slip rates but also on slip rate gradients. Following Fleck et al. (1994), the slip gradient in the slip direction is related to geometrically necessary edge dislocations, and a slip gradient in the transverse direction is related to geometrically necessary screw dislocations. Based on this, an effective slip measure, $\gamma_{\mathrm{e}}^{(\alpha)}$, depending on the slip and the slip gradients is introduced as

$$\dot{\gamma}_{\mathrm{e}}^{(\alpha)^2} = \dot{\gamma}^{(\alpha)^2} + \left(l_{\mathrm{S}} \dot{\gamma}_{,i}^{(\alpha)} s_i^{(\alpha)}\right)^2 + \left(l_{\mathrm{T}} \dot{\gamma}_{,i}^{(\alpha)} t_i^{(\alpha)}\right)^2 \tag{3}$$

where $t_i^{(\alpha)}$ is a unit vector in the transverse direction (with $\boldsymbol{t}^{(\alpha)} = \boldsymbol{s}^{(\alpha)} \times \boldsymbol{m}^{(\alpha)}$) and l_{S} and l_{T} are material length scales introduced for dimensional consistency. Here, $()_{,i} = \partial/\partial x_i$ is the spatial derivative. The principle of virtual power takes the form

$$\int_V \left(\sigma_{ij} \delta \dot{\epsilon}_{ij} + \sum_{\alpha} \left(Q^{(\alpha)} - \tau^{(\alpha)}\right) \delta \dot{\gamma}^{(\alpha)} + \sum\nolimits_{\alpha} \left(\xi_{\mathrm{S}}^{(\alpha)} s_i^{(\alpha)} + \xi_{\mathrm{T}}^{(\alpha)} t_i^{(\alpha)} \right) \delta \dot{\gamma}_{,i}^{(\alpha)} \right) \mathrm{d}V = \int_S \left(T_i \delta \dot{u}_i + \sum\nolimits_{\alpha} r^{(\alpha)} \delta \dot{\gamma}^{(\alpha)} \right) \mathrm{d}S \tag{4}$$

where $Q^{(\alpha)}$ is a stress field work conjugate to the slip rate, and the higher order stresses $\xi_{\mathrm{S}}^{(\alpha)}$ and $\xi_{\mathrm{T}}^{(\alpha)}$ are work conjugate to the slip rate gradients along the slip direction and the transverse direction, respectively. T_i is the stress traction and $r^{(\alpha)}$ denotes the higher order traction working on the boundary S. The Cauchy stress is denoted σ_{ij} and $\tau^{(\alpha)} = \sigma_{ij} \mu_{ij}^{(\alpha)}$ is the Schmid stress. The virtual power relation (4) is a special case of the virtual power relation in Gurtin (2002).

By use of an effective stress, denoted $\tau_{\mathrm{e}}^{(\alpha)}$, which is work-conjugate to the effective slip rate measure, $\dot{\gamma}_{\mathrm{e}}^{(\alpha)}$, constitutive equations are obtained for the effective stress $Q^{(\alpha)}$ and the higher order stresses $\xi_{\mathrm{S}}^{(\alpha)}$ and $\xi_{\mathrm{T}}^{(\alpha)}$ as

$$Q^{(\alpha)} = \tau_{\mathrm{e}}^{(\alpha)} \frac{\dot{\gamma}^{(\alpha)}}{\dot{\gamma}_{\mathrm{e}}^{(\alpha)}} \tag{5}$$

$$\xi_{\mathrm{S}}^{(\alpha)} = \tau_{\mathrm{e}}^{(\alpha)} \frac{\dot{\gamma}_{,i}^{(\alpha)} s_i^{(\alpha)}}{\dot{\gamma}_{\mathrm{e}}^{(\alpha)}} l_{\mathrm{S}}^2, \quad \xi_{\mathrm{T}}^{(\alpha)} = \tau_{\mathrm{e}}^{(\alpha)} \frac{\dot{\gamma}_{,i}^{(\alpha)} t_i^{(\alpha)}}{\dot{\gamma}_{\mathrm{e}}^{(\alpha)}} l_{\mathrm{T}}^2 \tag{6}$$

Then, the introduced stress $\tau_{\mathrm{e}}^{(\alpha)}$ can be expressed in the following quadratic form

$$\tau_{\mathrm{e}}^{(\alpha)^2} = Q^{(\alpha)^2} + l_{\mathrm{S}}^{-2} \xi_{\mathrm{S}}^{(\alpha)^2} + l_{\mathrm{T}}^{-2} \xi_{\mathrm{T}}^{(\alpha)^2} \tag{7}$$

The viscous material behavior is modeled by use of a power-law creep model formulated as

$$\dot{\gamma}_{\mathrm{e}}^{(\alpha)} = \dot{\gamma}_0 \left(\frac{\tau_{\mathrm{e}}^{(\alpha)}}{g^{(\alpha)}} \right)^{1/m} \tag{8}$$

where $\dot{\gamma}_0$ is a reference slip rate and m is a strain rate hardening index. The slip resistances $g^{(\alpha)}$ characterize the current strain hardened state of the crystal, and harden from an initial value τ_0 according to

$$\dot{g}^{(\alpha)} = \sum_{\beta} h_{\alpha\beta} \dot{\gamma}_{\mathrm{e}}^{(\beta)}, \quad h_{\alpha\beta} = h\delta_{\alpha\beta} + ph\left(1 - \delta_{\alpha\beta}\right) \tag{9}$$

Here, p is the latent hardening index, $\delta_{\alpha\beta}$ denotes the Kronecker delta function, and h is the self-hardening modulus given empirically by

$$h(\gamma_{\mathrm{a}}) = h_0 \Big/ \cosh\left(\frac{h_0 \gamma_{\mathrm{a}}}{\tau_{\mathrm{s}} - \tau_0} \right), \quad \gamma_{\mathrm{a}} = \sum_{\alpha} \int \dot{\gamma}_{\mathrm{e}}^{(\alpha)} \mathrm{d}t \tag{10}$$

where the constant h_0 represents an initial hardening rate, τ_{s} is a saturation stress, and γ_{a} is the accumulated effective slip.

3. Numerical method

The numerical solutions are obtained using the finite element method. The slip rate increments are taken as nodal degrees of freedom on an equal footing with the displacement increments. These primary unknowns are interpolated within each element between nodal increments as

$$\Delta u_i = \sum_{N=1}^{2k} N_i^N \Delta D^N, \quad \Delta \dot{\gamma}^{(\alpha)} = \sum_{N=1}^{l} M^N \Delta \dot{\gamma}_N^{(\alpha)} \tag{11}$$

where N_i^N and M^N are shape functions and k and l are the number of nodes used for the interpolations. For this plane strain study, the elements used for the displacements are 8-node quadrilaterals with quadratic shape functions, and the elements used for interpolation of the slip rate increments are 4-node quadrilaterals with linear shape functions, i.e., $k = 8$ and $l = 4$. The integrations are carried out using 2×2 point Gaussian integration for both element types. To ensure the integration points for the two element types to coincide, the same Jacobian is used for both element types.

The specimen considered in this study is shown in Fig. 1. It is a square ($a_0 = b_0$) single hexagonal close packed crystal containing a cylindrical void in the center with a diameter of one tenth of the side length ($r_0 = 0.1a_0$). The axis of the cylindrical void is chosen to be parallel to the basal plane normal [0001] as in Gan and Kysar (2007). The three active slip systems, each oriented at the angle 60° with respect to the others, are also shown in Fig. 1.

For a local material it is possible to consider only a quarter of the crystal due to symmetry, whereas for the nonlocal material the higher order boundary conditions make such an approach difficult. In this study the full crystal is considered for all analyses. The boundary conditions applied to the single crystal are given by

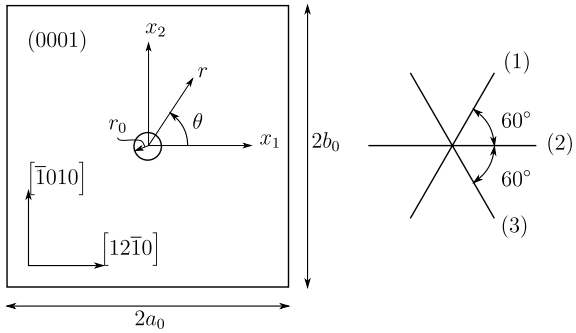

Fig. 1. Cylindrical void in an HCP single crystal showing coordinate systems, dimensions, slip systems and crystallographic orientation.

$$\begin{aligned} &\dot{u}_1 = 0, \quad \dot{T}_2 = 0 \ \text{ at } x_1 = -a_0 \\ &\dot{u}_1 = \dot{U}_1, \quad \dot{T}_2 = 0 \ \text{ at } x_1 = a_0 \\ &\dot{u}_2 = 0, \quad \dot{T}_1 = 0 \ \text{ at } x_2 = -b_0 \\ &\dot{u}_2 = \dot{U}_2, \quad \dot{T}_1 = 0 \ \text{ at } x_2 = b_0 \end{aligned} \tag{12}$$

where $\dot{T}_i$ are surface traction rates and $\dot{U}_i$ are the prescribed end displacement rates. Furthermore, the higher order boundary conditions are applied as vanishing higher order tractions, $r^{(\alpha)} = 0$, on the four external edges and on the void surface. Another possibility for the higher order boundary conditions is to let the slips vanish, i.e., letting the boundaries be impenetrable to dislocations. That would be appropriate at a stiff inclusion but not for a void. The mesh used for the presented results consists of 16,224 elements and is finest at the void surface with 312 elements around the void.

For the plane strain problem considered, with in-plane slip systems, there are no slip gradients in the transverse direction, and therefore the length scale parameter, l_{T}, has no influence on the results. The other length scale parameter, l_{S}, is denoted l in the following.

4. Results

The material parameters used in the calculations are Young's modulus, $E = 63.9$ GPa, Poisson's ratio, $\nu = 0.36$, initial slip resistance, $\tau_0 = 1$ MPa, reference slip rate, $\dot{\gamma}_0 = 0.001\ \mathrm{s}^{-1}$, and strain rate hardening index, $m = 0.03$. Results using the local constitutive formulation are presented both with and without strain hardening. For the results with hardening the following hardening parameters are used: self-hardening modulus, $h_0 = E/100$, saturation stress, $\tau_{\mathrm{s}} = 1.8\tau_0$, and latent hardening index, $p = 1.0$. All the presented results using the non-local formulation are without strain hardening, i.e., $h_0 = 0$. The prescribed end displacement rates are given by $\dot{U}_1/(2a_0) = \dot{U}_2/(2a_0) = 0.0001\ \mathrm{s}^{-1}$. The results presented in this section are taken at the deformation state given by $U_1/(2a_0) = U_2/(2a_0) = 3.5 \times 10^{-5}$.

Contours of slip in the three slip systems and the total slip, $\gamma_{\mathrm{tot}} = \gamma^{(1)} + \gamma^{(2)} + \gamma^{(3)}$, are shown in Fig. 2 for a non-hardening local material, i.e., using the internal material length scale $l = 0$ and the hardening modulus

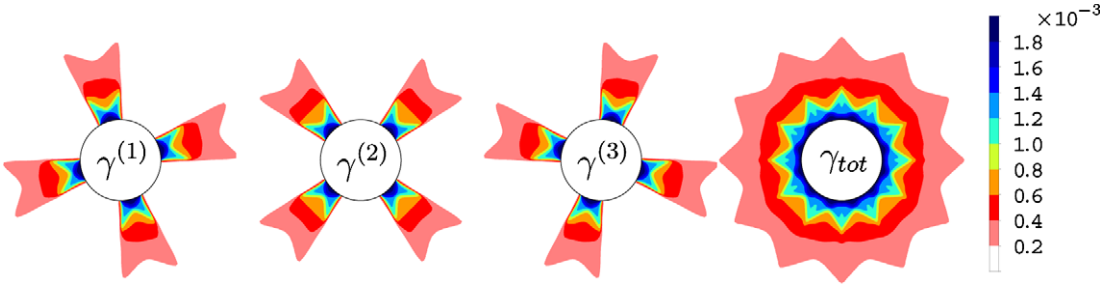

Fig. 2. Contours of slip in the three slip systems using a local formulation without hardening ($l = 0$, $h_0 = 0$).

$h_0 = 0$. It is seen that the slip contours are periodic with a period of 90°. Slip system one is mostly active in the region $0 \leqslant \theta \leqslant 30°$, slip system two is mostly active in the region $30° \leqslant \theta \leqslant 60°$, and slip system three is mostly active in the region $60° \leqslant \theta \leqslant 90°$ of the upper right quadrant. The location of angular sectors with only one effective slip system is as predicted by anisotropic slip line theory in Gan and Kysar (2007), where they are denoted as *slip sectors*.

The slip contours using a local formulation with hardening are shown in Fig. 3. The slip sectors are very similar to the results for the non-hardening material, except that the magnitudes of the accumulated slips are less than for the non-hardening case.

Fig. 4 shows the slip in the three slip systems and the total slip, $\gamma_{\text{tot}} = \gamma^{(1)} + \gamma^{(2)} + \gamma^{(3)}$, plotted along the path $r/r_0 = 1.0$ for a non-hardening local material. It can be seen that the boundaries between two active slip sectors around $\theta = 0°$, 30°, 60° etc. are very thin. Within each slip sector the level of slip is almost constant along the void surface. The analogous plot is shown in Fig. 5 for a hardening local material. Here, the slip sector boundaries are also very thin as for the non-hardening local material.

Stress contours expressed in polar coordinates (σ_{rr}, $\sigma_{\theta\theta}$ and $\sigma_{r\theta}$) are shown in Fig. 6 for the non-hardening local material. The left column shows contours over the entire specimen, and the right column shows contours in the vicinity of the void. The results are very similar to those obtained by Gan and Kysar (2007) using anisotropic slip line theory for a rigid-ideally plastic crystal. However, here we have edge effects and purely elastic deformations far from the void, so the results are only directly comparable near the void. The radial stress, σ_{rr}, has a 12-point 'star' structure, whereas the circumferential stress, $\sigma_{\theta\theta}$, has a more smooth variation. The magnitude of the polar shear stress, $\sigma_{r\theta}$, is much smaller than the two other stress components and displays an interesting pattern with alternating positive and negative values. In addition, the anisotropic slip line theory solution predicts values of $\sigma_{r\theta}$ that are periodic with angle on logarithmic spirals which emanate from the void surface.

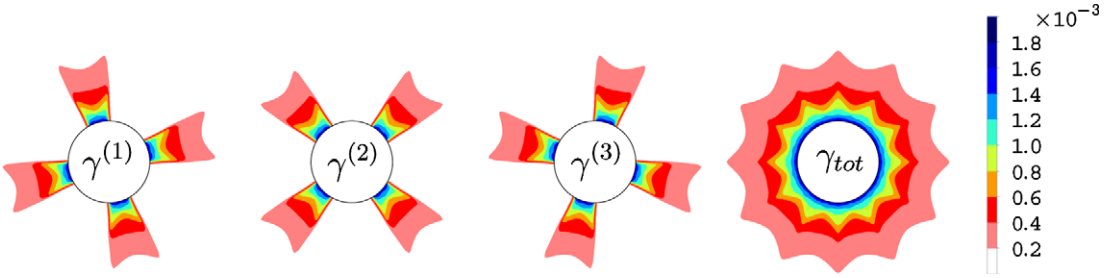

Fig. 3. Contours of slip in the three slip systems using a local formulation with hardening ($l = 0$, $h_0 = E/100$).

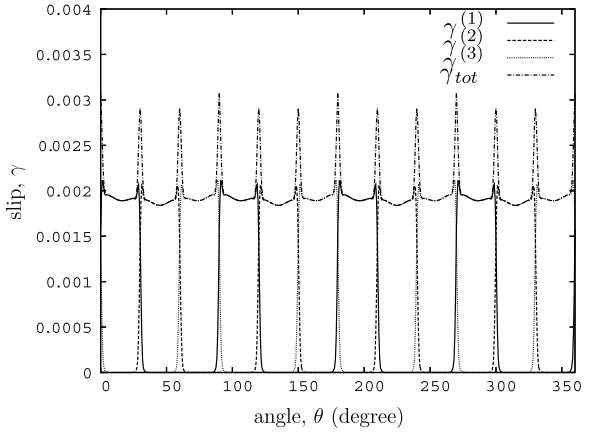

Fig. 4. Slip along the path $r/r_0 = 1.0$ using a local formulation without hardening.

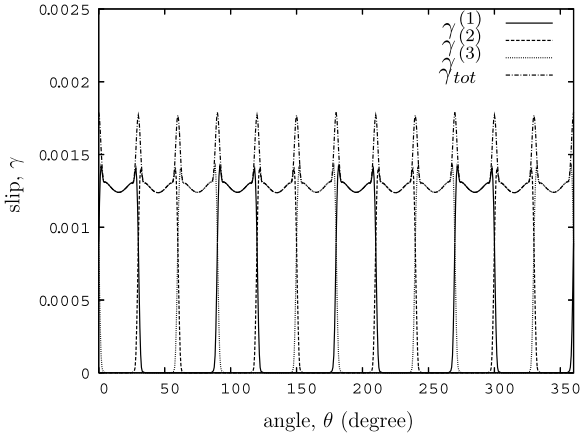

Fig. 5. Slip along the path $r/r_0 = 1.0$ using a local formulation with hardening.

Fig. 7 shows the stress components expressed in Cartesian coordinates along the path $r/r_0 = 1.0$ for the non-hardening local material; they are periodic with a period of 180°. The shear stress is constant, $|\sigma_{12}/\tau_0| \approx 1.08$, within the slip sectors where slip system two is active. The slip line solution (Gan and Kysar, 2007) predicts $|\sigma_{12}/\tau_0| = 1.0$ in these slip sectors. This difference is mainly due to the viscoplastic effects in the present formulation which are not accounted for in the analytical slip line solution. In Fig. 8 the stress components expressed in polar coordinates are plotted along the path $r/r_0 = 1.0$. As expected, the radial stress component, σ_{rr}, and the polar shear stress component, $\sigma_{r\theta}$, vanish at the void surface. The average circumferential stress, $\sigma_{\theta\theta}$, on the surface of the void predicted from simulation is close to $2.3\tau_0$, while the slip line solution predicts an average normalized circumferential stress of $6\ln(3)/\pi \approx 2.098$. The value of $\sigma_{\theta\theta}$ is periodic with a period of 30° which is also evident from the contour plots of $\sigma_{\theta\theta}$ in Fig. 6. At the radius $r/r_0 = \sqrt{3}$ the slip line solution predicts $\sigma_{rr}/\tau = 2/\sqrt{3} \approx 1.155$ and $\sigma_{r\theta} = 0$. Also, the circumferential stress, $\sigma_{\theta\theta}$, is expected to vary in the same way as on the void surface. The stresses in polar coordinates from the simulation along the path $r/r_0 = \sqrt{3}$ are plotted for the non-hardening local material in Fig. 9. The radial shear stress vanishes at all angles for that radius as predicted and the radial stress has the average value $\sigma_{rr}/\tau_0 \approx 1.17$.

The slip contours shown in Fig. 10 for a non-local material with void size relative to the material length scale $r_0/l = 10$ are somewhat different than the results for the local material shown in Fig. 2. The magnitudes of the slips are approximately the same which indicates only a very small gradient contribution to the effective slip. The main difference though is that the slip contours are no longer symmetric about the radial center line in each slip sector. This result is not unexpected. Classical continuum single crystal plasticity theory for infinitesimal deformation gradients is invariant to an interchange of the unit lattice vectors $s_i^{(\alpha)}$ and $m_i^{(\alpha)}$. This can be seen in the definition of the Schmid tensor (1) and its subsequent use in the development of the infinitesimal theory in which lattice rotations are negligible. As a consequence of this invariance and the symmetry of the slip systems, the slip distribution about the radial center line of each slip sector is symmetric in spite of the fact that only one effective slip system is active in that region. (N.B. The simulations employ a finite deformation formulation, however the accumulated slips are sufficiently small so that the computed lattice rotation is negligible.) Introduction of the effective slip measure $\gamma_e^{(\alpha)}$ in (3) breaks this symmetry because the directions $s_i^{(\alpha)}$ and $m_i^{(\alpha)}$ are treated differently. Indeed it can be seen for the non-local hardening case in Fig. 10 that the slip gradients in the slip directions are smaller than the slip gradients in the directions normal to the slip planes which can be explained as a consequence of the differences in contributions of slip gradients in the slip directions and slip plane normal directions to the internal plastic work. The reduction of symmetry is also evident in that the slip contours for the non-local material are periodic with a period of 180°, whereas the slip contours in Fig. 2 for the local material have a period of 90°.

The slip contours for a non-local material with a small void size – here taken to be $r_0/l = 1$ and shown in Fig. 11 – are very different from the results for the local material shown in Fig. 2 and also from the non-local material with a larger void size, $r_0/l = 10$, in Fig. 10. All slip occurs in localized bands in the slip directions, so

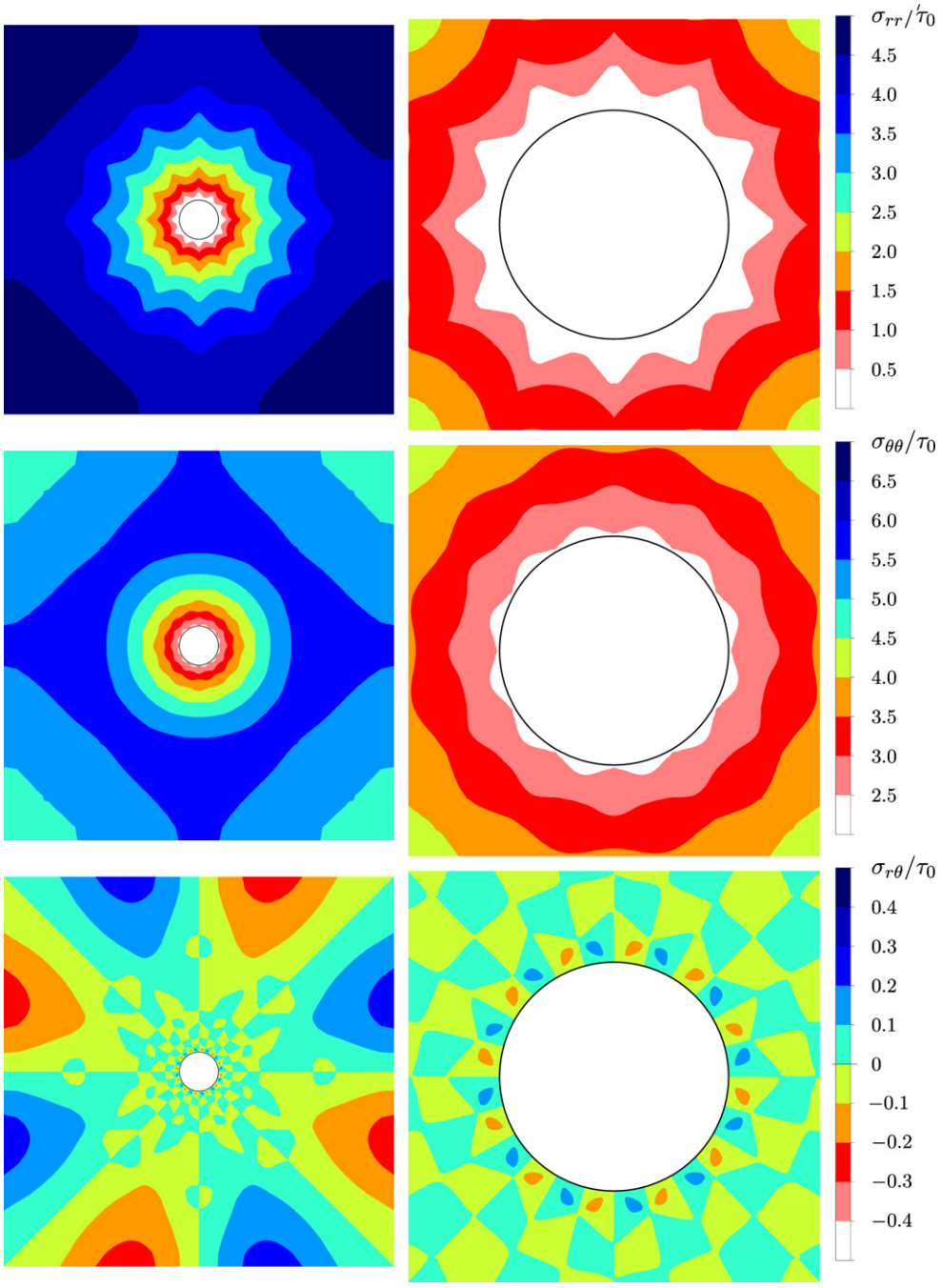

Fig. 6. Contours of stresses expressed in polar coordinates for a non-hardening local material.

the slip gradients in the slip directions are much smaller than the slip gradients in the directions normal to the slip planes. Again the symmetry is broken and it is notable that the magnitude of slip is significantly lower than for the other cases. The plastic slip is localized near the void surface, and as before the smallest magnitude of slip gradient is in the direction of slip rather than the transverse direction.

It is interesting to note that the plastic slip contours for the case of $r_0/l = 1$ bear a resemblance to the slip expected due to dislocation emission and motion from a cylindrical void by Lubarda et al. (2004) in an analytical study. In that work, the void is assumed to exist in an initially dislocation-free crystal so that any plastic

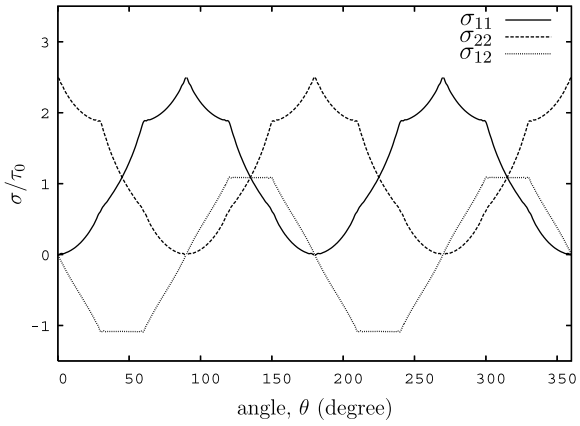

Fig. 7. Stress components in Cartesian coordinates along the path $r/r_0 = 1.0$ for a local material without hardening.

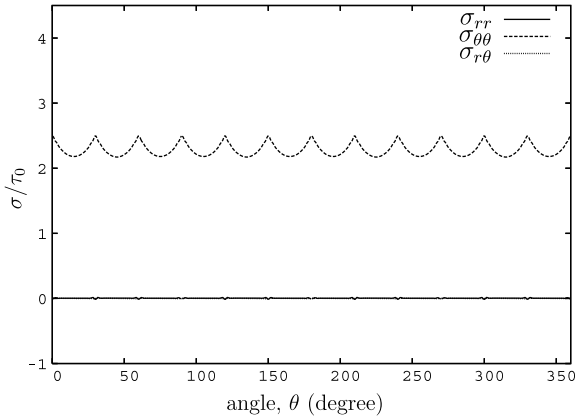

Fig. 8. Stress components in polar coordinates along the path $r/r_0 = 1.0$ for a local material without hardening.

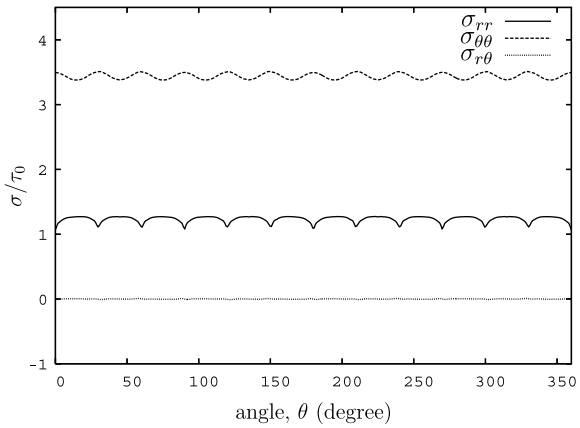

Fig. 9. Stress components in polar coordinates along the path $r/r_0 = \sqrt{3}$ for a local material without hardening.

deformation must be due to dislocations nucleated from the void surface. Similarly, for the high strain gradient case in the present study, the strain gradients lead to very rapid hardening response which would tend to "shut down" the active slip systems, allowing only those slip systems which can operate under relatively low

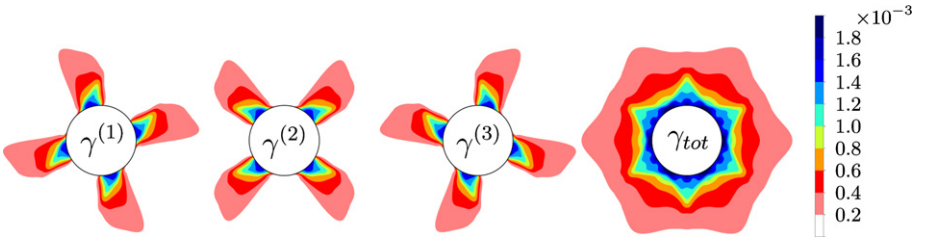

Fig. 10. Contours of slip in the three slip systems for a non-local material with $r_0/l = 10$.

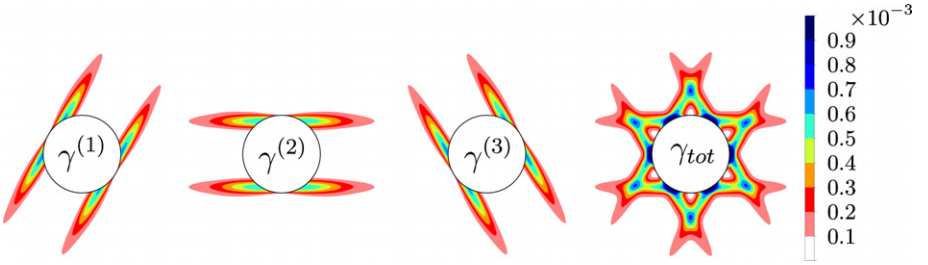

Fig. 11. Contours of slip in the three slip systems for a non-local material with $r_0/l = 1$.

gradients of slip to become active. It should be noted that there is an important difference between the analytical predictions of Lubarda et al. (2004) and the results herein. In the dislocation emission analyses, the presumed active dislocation is that with a slip direction which intersects the void surface with an angle of 45°, which is not the case in the present simulations.

Fig. 12 shows slip sector boundaries (areas with double slip), defined as areas where the slip magnitudes in at least two slip systems are higher than 10^{-4}. It can be seen that the slip sector boundaries are very similar for the hardening and the non-hardening local formulation. This is to be expected since the introduction of hardening in a local formulation does not break the invariance due to interchange of $s_i^{(\alpha)}$ and $m_i^{(\alpha)}$ of the kinematical structure and constitutive relations for the case of infinitesimal deformation gradients, which is effectively the case for the very modest magnitudes of strain encountered in these simulations. The reduced symmetry for the case of non-local formulation manifests itself in a broadened slip sector boundary for the void size $r_0/l = 10$. It is presumed that the enhanced local hardening associated with the region of double slip might serve to further modify the sector boundary structure around a void, an effect which is not modelled in the present simulation. Finally the significant change in slip behavior associated with the small void size case $r_0/l = 1$ is evident in Fig. 12.

The slips around the void surface are plotted in Fig. 13 for the void size $r_0/l = 10$. The slip magnitudes are significantly lower than the slip magnitudes for the local material shown in Fig. 4, and also the curves are smoother in the non-local case. Another significant difference is that the slip sector boundaries are much wider

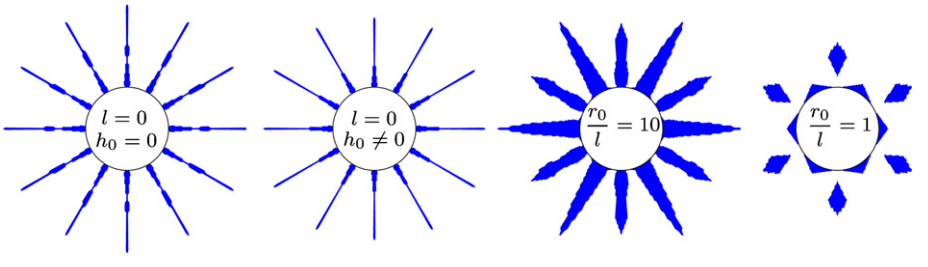

Fig. 12. Areas with double slip for the local formulation with and without hardening and for two void sizes using the non-local formulation.

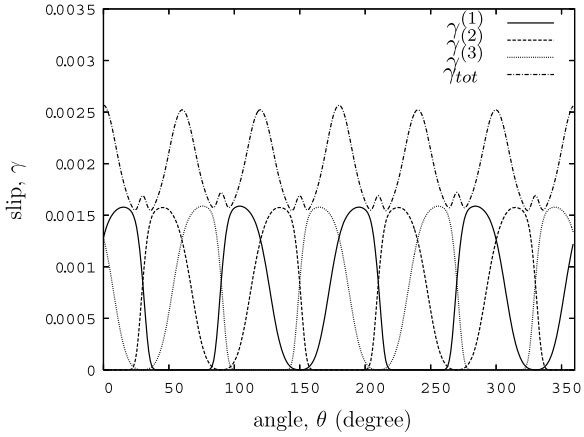

Fig. 13. Slip along the path $r/r_0 = 1.0$ for a non-local material with void size $r_0/l = 10$.

than for the local material (as shown in Fig. 12), and there are even areas where all three slip systems are active; however, within these areas of triple slip the slip magnitude on one of the three slip systems is very small. Fig. 14 shows the slips around the void surface for the void size $r_0/l = 1$. It can be seen that there are large variations in the total slip around the void surface; there are even material points which suffer almost no plastic deformation.

Contours of stresses expressed in polar coordinates for the non-local material with void size $r_0/l = 10$ are shown in Fig. 15 and can be compared to those for the local material in Fig. 6. The reduction in symmetry from 12-fold to sixfold rotation is evident around the void. Two points stand out. One is that the magnitude of the stress components does not change dramatically from that of the local non-hardening case for the void size $r_0/l = 10$. In addition, as discussed above, the slip line solution predicts that $\sigma_{r\theta} = 0$ and $\sigma_{rr} =$ constant on $r/r_0 = \sqrt{3}$ so that the stress field exhibits self-similarity in the radial direction for a non-hardening local crystal. The contours of $\sigma_{r\theta}$ in Fig. 15, though, demonstrate that the radial self-symmetry is lost in addition to a reduction of the rotational symmetry. The polar stress contours are shown in Fig. 16 for the small void sizes ($r_0/l = 1$). The stresses exhibit a sixfold rotational symmetry and the magnitudes are larger.

The stresses expressed in Cartesian coordinates for the larger void size ($r_0/l = 10$) are shown in Fig. 17 along the path given by $r/r_0 = 1.0$. It is seen that the shear stress, σ_{12}, is not constant in the sectors where slip system two is active as it was the case for the local material. Fig. 18 shows the stress components expressed in polar coordinates for the non-local case with $r_0/l = 10$ along the path given by $r/r_0 = 1.0$. The radial stress and the

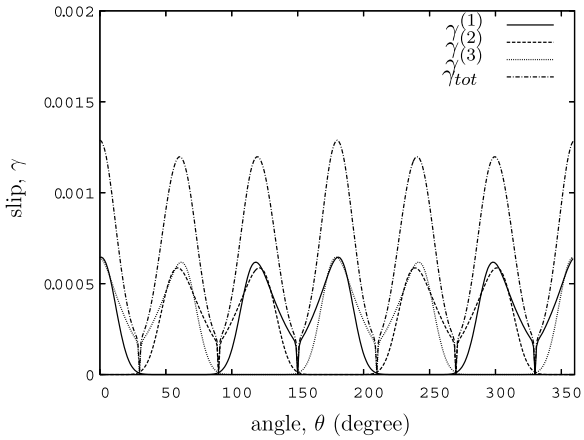

Fig. 14. Slip along the path $r/r_0 = 1.0$ for a non-local material with void size $r_0/l = 1$.

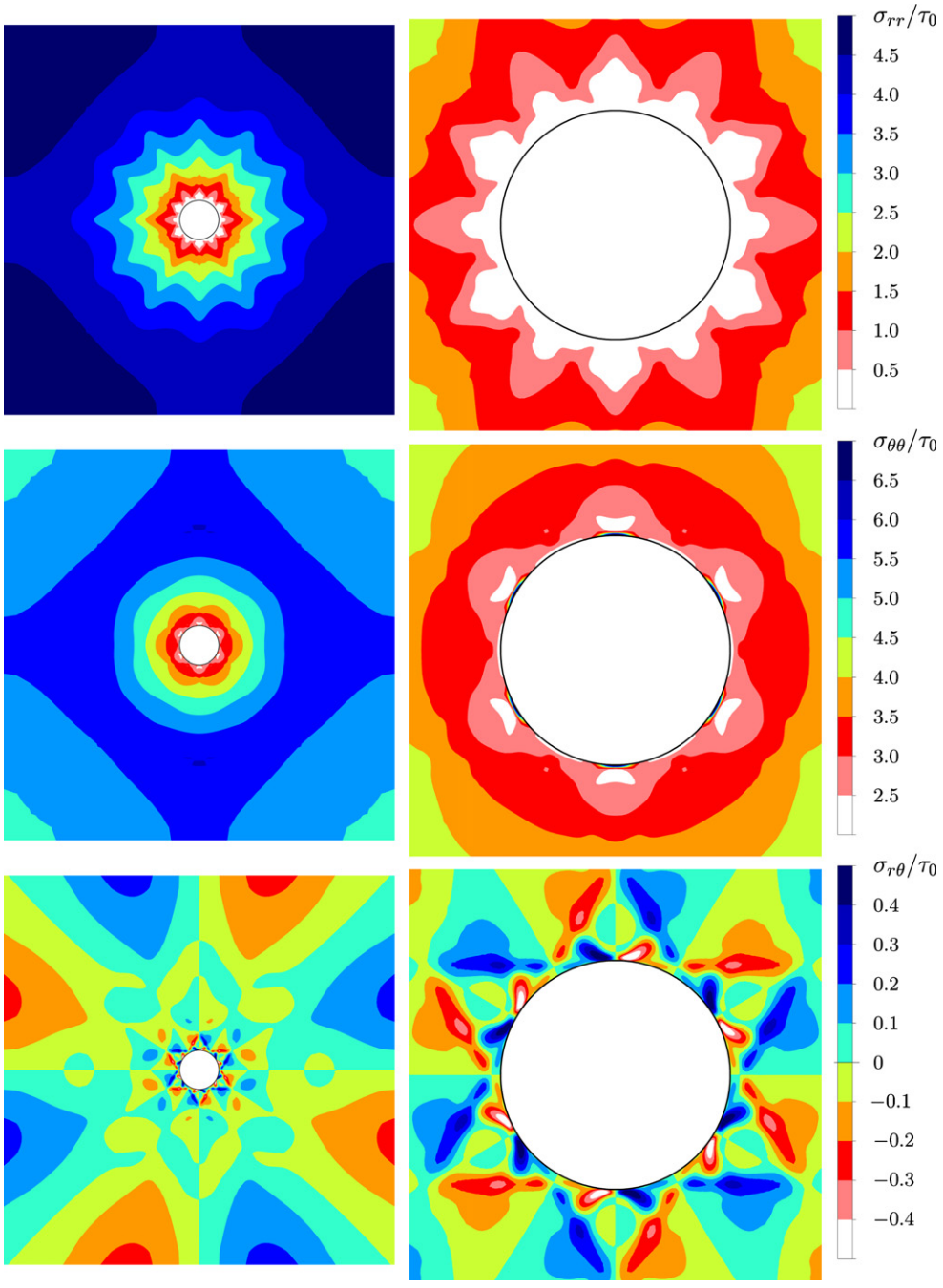

Fig. 15. Contours of stresses expressed in polar coordinates for a non-local material with void size $r_0/l = 10$.

polar shear stress both vanish at the void surface. The circumferential stress, $\sigma_{\theta\theta}$, has its peaks near $\theta = 30°$, 90°, 150°, 210°, 270° and 330°. The stress level of the peaks is about $10\tau_0$, whereas the circumferential stress for the local material varies between approximately $2.1\tau_0$ and $2.5\tau_0$. Thus even the larger void sizes ($r_0/l = 10$) can dramatically increase the necessary stress level on the void surface to effect plastic deformation. It is interesting to note that the regions of high $\sigma_{\theta\theta}$ do not extend very far radially from the void surface into the surrounding crystal, and that these regions are separated by regions which have a zero $\sigma_{\theta\theta}$ which implies that the material in these regions on the void surface are devoid of stress.

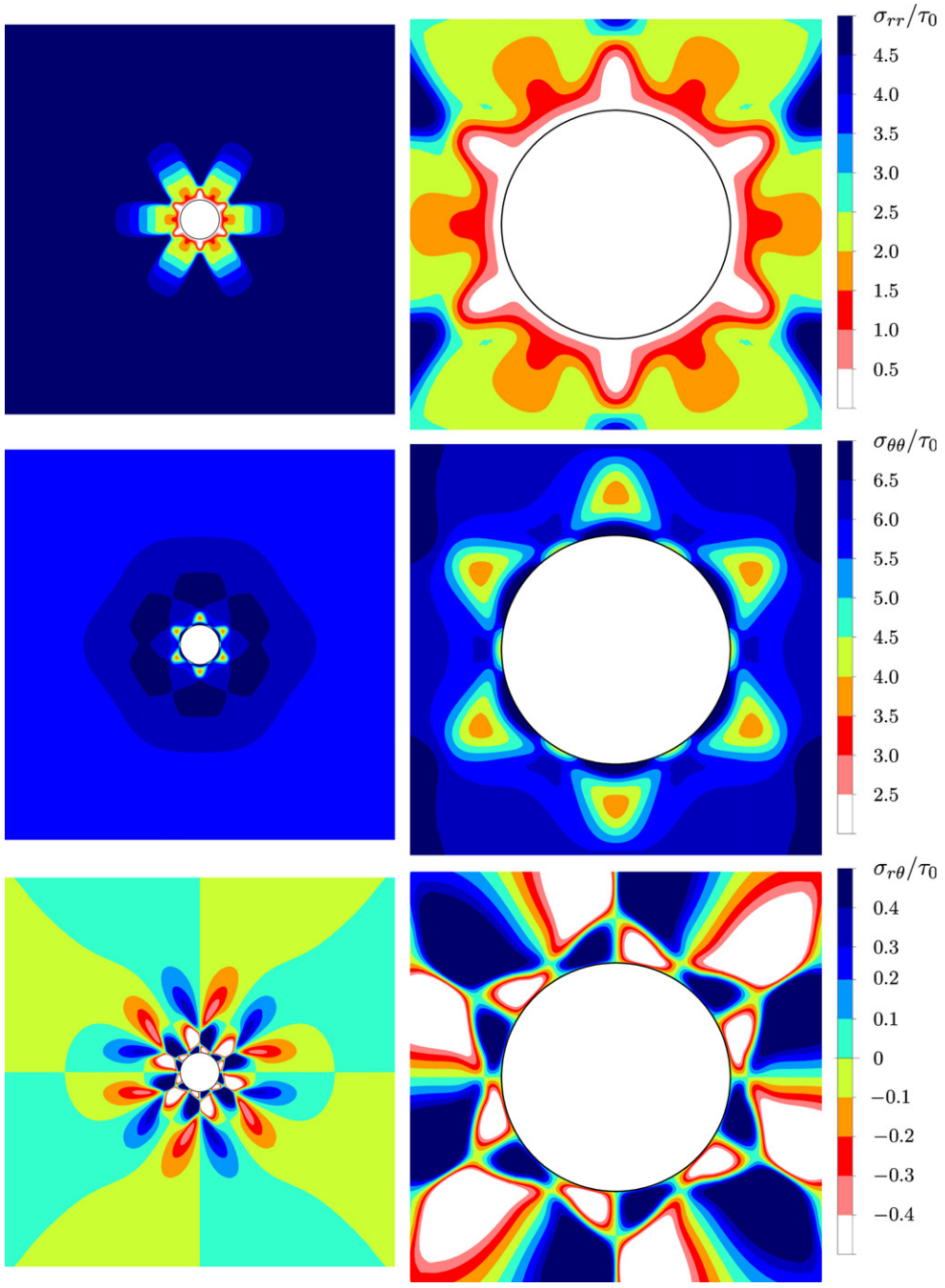

Fig. 16. Contours of stresses expressed in polar coordinates for a non-local material with void size $r_0/l = 1$.

For the case of small voids ($r_0/l = 1$), the stresses exhibit a sixfold rotational symmetry and the magnitudes are larger. The stresses on the void surface are shown in Fig. 19. Again the radial stress and the shear stress vanish, whereas the circumferential stress varies between approximately $4\tau_0$ and $12\tau_0$. Thus, there are no material points around the void surface with zero stress as there were with the void size $r_0/l = 10$.

Fig. 20 shows the equibiaxial stress level, σ, at which plastic deformation initiates as a function of the void size. The initiation of plastic deformation is here defined as the far-field stress level where the effective shear stress, $\tau_e^{(\alpha)}$, exceeds the slip resistance, τ_0, in any part of the crystal. For a void in an elastic medium subjected

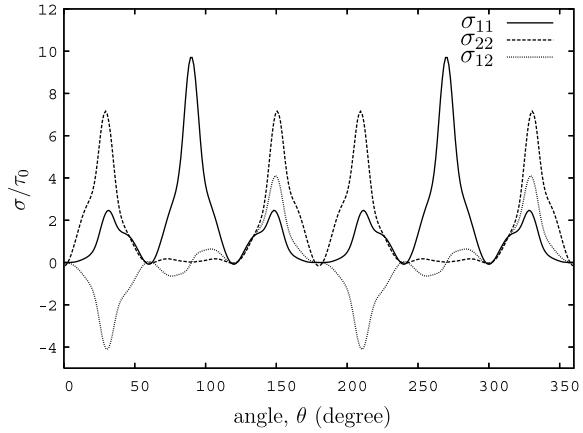

Fig. 17. Stress components in Cartesian coordinates along the path $r/r_0 = 1.0$ for a non-local material with $r_0/l = 10$.

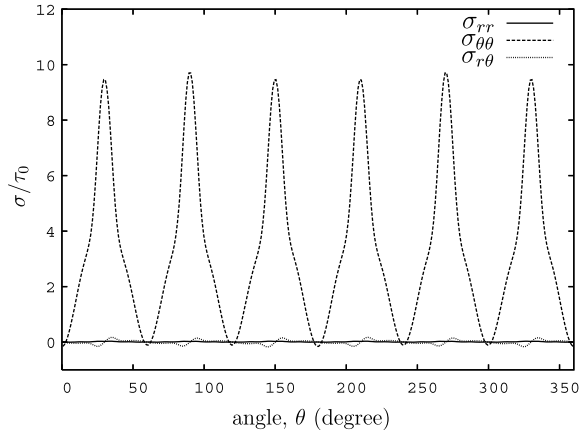

Fig. 18. Stress components in polar coordinates along the path $r/r_0 = 1.0$ for a non-local material with $r_0/l = 10$.

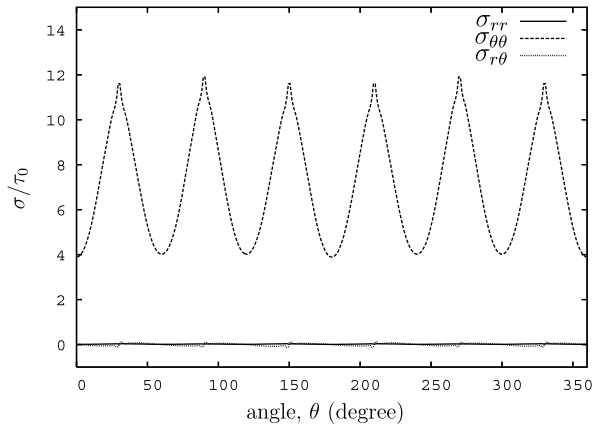

Fig. 19. Stress components in polar coordinates along the path $r/r_0 = 1.0$ for a non-local material with $r_0/l = 1$.

to an equibiaxial tensile stress, σ, applied at a remote distance from the void, the analytical stress solution at the void surface predicts a circumferential stress $\sigma_{\theta\theta} = 2\sigma$ and vanishing radial and polar shear stresses. The resolved shear stress on a slip system is highest when the circumferential stress direction is 45° from the slip

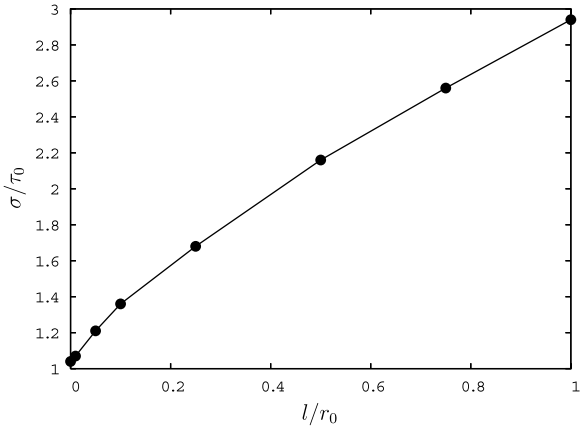

Fig. 20. The overall equibiaxial stress level, σ, that causes an effective stress $\tau_e > \tau_0$ as a function of the void size.

direction. In that case, the resolved shear stress, $\tau^{(\alpha)}$, equals half the circumferential stress ($\tau^{(\alpha)} = \sigma$). Thus, for a local material where $\tau_e^{(\alpha)} = \tau^{(\alpha)}$ purely elastic considerations predict that plastic deformation initiates at $\sigma/\tau_0 \approx 1$. Furthermore, the slip line solution predicts the average value of $\sigma_{\theta\theta}$ around the void surface at which plastic deformation has initiated at all angles as $3\ln(3)\tau/\pi \approx 1.049\tau$. It is seen in Fig. 20 that this is in fact the case for $l = 0$. When the void size is decreased relative to the material length scale, the stress level required to initiate plastic deformation is increased. For a void radius, r_0, equal to the internal material length scale, l, the required stress level has increased to approximately three times the slip resistance.

5. Conclusions

The goal of this study is to study the influence of hardening and void size on the stress and deformation fields around a cylindrical void in a single crystal. Hardening within the framework of a local constitutive formulation is considered which corresponds physically to an accumulation of statistically stored dislocations. In addition, strain gradient effects within the framework of a non-local constitutive formulation is considered, which corresponds physically to a segregation of geometrically necessary dislocations. A combination of strain hardening and strain gradient effects is not considered in this study.

The results show that the introduction of hardening in the local constitutive relationship has very little effect on the slip fields around the void when compared to the case of a non-hardening local material. The overall extent of the angular sectors of single slip is unaffected, but the magnitude of the slip is decreased.

When a non-local constitutive relation is used, however, the results are significantly different from the non-hardening local case. For the case of void size $r_0/l = 10$, the boundaries between the angular slip sectors broaden so that there are regions in which multiple slip systems are activated simultaneously. The magnitudes of the slip change very little between the two cases.

For the case of small void size ($r_0/l = 1$), the form of the deformation field changes dramatically. The deformation localizes into regions which intersect the void surface and are parallel to the slip system. This localization is reminiscent of the type of dislocation activity associated with dislocation nucleation from a void in a crystal which is free of dislocations or other dislocation sources as discussed in Lubarda et al. (2004).

Finally, the applied stress state to activate plastic deformation around the void associated with the non-local material can be as high as three times that of the non-hardening local case. The study by Kysar et al. (2005) concluded that the stress state necessary to activate plastic deformation in face centered cubic crystals can be up to 50% higher than that of an isotropic material, however there was very little difference for hexagonal closed packed crystals (Gan and Kysar, 2007). This discrepancy exists because the effective Schmid factors for the slip systems of a hexagonal close packed crystal are higher than the analogous Schmid factors for the slip systems of a face centered cubic crystal. Therefore, one can conclude that the anisotropy of the material properties as well as the non-local constitutive formulation act to increase the externally applied stress

required to activate void growth in single crystals. This has potential implications in the development of theories of effective porous media which are used to model crack growth in ductile materials.

Acknowledgements

The work of U.B. is financially supported by the Danish Technical Research Council in a project entitled Modeling Plasticity at the Micron Scale. J.W.K. acknowledges support from AFOSR FA9550-06-1-0214. The authors express gratitude for stimulating conversations with Christian F. Niordson and Viggo Tvergaard.

References

Ahn, D.C., Sofronis, P., Minich, R., 2006. On the micromechanics of void growth by prismatic-dislocation loop emission. J. Mech. Phys. Solids 54 (4), 735–755.

Borg, U., in press. Strain gradient crystal plasticity effects on flow localization, Int. J. Plasticity., doi:10.1016/j.ijplas.2007.01.003.

Fleck, N.A., Hutchinson, J.W., 2001. A reformulation of strain gradient plasticity. J. Mech. Phys. Solids 49, 2245–2271.

Fleck, N.A., Muller, G.M., Ashby, M.F., Hutchinson, J.W., 1994. Strain gradient plasticity: theory and experiment. Acta Metall. Mater. 42, 475–487.

Fredriksson, P., Gudmundson, P., 2005. Size-dependent yield strength of thin films. Int. J. Plast. 21, 1834–1854.

Gan, Y.X., Kysar, J.F., 2007. Cylindrical void in a rigid-ideally plastic single crystal III: hexagonal close-packed crystal. Int. J. Plast. 23, 592–619.

Gan, Y.X., Kysar, J.F., Morse, T.L., 2006. Cylindrical void in a rigid-ideally plastic single crystal II: experiments and simulations. Int. J. Plast. 22, 39–72.

Gurtin, M.E., 2002. A gradient theory of single-crystal viscoplasticity that accounts for geometrically necessary dislocations. J. Mech. Phys. Solids 50, 5–32.

Hussein, M.I., Borg, U., Niordson, C.F., Deshpande, V.S., in press. Plasticity size effects in voided crystals, in press.

Koplik, J., Needleman, A., 1988. Void growth and coalescence in porous plastic solids. Int. J. Solids Struct. 24, 835–853.

Kysar, J.F., Gan, Y.X., Mendez-Arzuza, G., 2005. Cylindrical void in a rigid-ideally plastic single crystal. part I: anisotropic slip line theory solution for face-centered cubic crystals. Int. J. Plast. 21, 1481–1520.

Lubarda, V.A., Schneider, M.S., Kalantar, D.H., Remington, B.A., Meyers, M.A., 2004. Void growth by dislocation emission. Acta Mater. 52 (6), 1397–1408.

Niordson, C.F., Redanz, P., 2004. Size-effects in plane strain sheet-necking. J. Mech. Phys. Solids 52, 2431–2454.

Peirce, D., Asaro, R.J., Needleman, A., 1983. Material rate dependence and localized deformation in crystalline solids. Acta Metall. 31, 1951–1976.

Stevens, A.L., Davison, L., Warren, W.E., 1972. Spall fracture in aluminum monocrystals – dislocation-dynamics approach. J. Appl. Phys. 43 (12), 4922–4927.

Tvergaard, V., 1990. Material failure by void growth to coalescence. Adv. Appl. Mech. 27, 83–151.